Advances in Colloid and Interface Science 319 (2023) 102963

Contents lists available at ScienceDirect

Advances in Colloid and Interface Science

journal homepage: www.elsevier.com/locate/cis

Historical Perspective

Nickel-based catalysts for electrolytic decomposition of ammonia towards hydrogen production

Justyna Łuczak *, Marek Lieder *

Department of Process Engineering and Chemical Technology, Faculty of Chemistry, Gdańsk University of Technology, Narutowicza 11/12, 80-233 Gdańsk, Poland

ARTICLE INFO

Keywords:
Ammonia oxidation reaction
Nickel-based electrodes
Electrocatalysis
Electrolysis of ammonia
Hydrogen production

ABSTRACT

Nickel is an attractive metal for electrochemical applications because it is abundant, cheap, chemically resilient, and catalytically active towards many reactions. Nickel-based materials (metallic nickel, its alloys, oxides, hydroxides, and composites) have been also considered as promising electrocatalysts for ammonia oxidation. The electrolysis of ammonia aqueous solution results in evolution of gaseous hydrogen and nitrogen. Up to date studies showed that metallic Ni and Ni (hydro)oxides are not catalytically active unless they are electrochemically converted to NiOOH at ~1.3 V *vs.* RHE. Then, dehydrogenation of NH_3 begins with electron coupled proton transfer to NiOOH resulting in a would-be reversible reduction of the latter to $Ni(OH)_2$. Unlike the water electrolysis process, in which solely oxygen is obtained at the anode, during ammonia electrooxidation apart from release of N_2, many undesired oxygenated nitrogen moieties may also turn up. These products appear after at least partial dehydrogenation of ammonia. Studies on NiOOH activity have been conducted for systems containing various modifiers, *e.g.*, Cu, Co, S, P, however, their particular role in catalytic activity has not yet been elucidated. Nowadays research is being conducted in the direction of increasing the activity, selectivity, and stability of NiOOH.

In this review, the electroactivity of Ni is analyzed and discussed in accordance with its oxidation states along with the ammonia oxidation mechanism. The main research problems to be solved and challenges for the future industrial use of ammonia are presented.

1. Introduction

According to the EU's hydrogen strategy (COM/2020/301), the priority for the EU is to develop hydrogen production technologies employing electrolyzers powered by renewable energy. This is main solution for decarbonizing various industrial sectors. Widespread production of green hydrogen will be possible if it is cheaper than producing hydrogen from fossil fuels. This means that the cost of the electrolyzer and its operation must be lowered. Electrodes used in industrial electrolyzers for hydrogen production are made of catalysts based on noble metals, which are rare, thus expensive.

Typical systems for water electrolysis produce hydrogen on cathode and oxygen on anode. The cathodic hydrogen evolution process (HER) has been well developed, whereas the oxygen evolution reaction (OER) poses many practical obstacles, mainly resulting from its high overpotential (low energy efficiency) and the hazard of H_2-O_2 mixture explosion. In this regard, replacing oxygen evolution with ammonia oxidation reaction (AOR) is a promising solution to tackle these obstacles. Namely, it has a very low redox potential $E^o = -0.097$ V *vs.* RHE [1], and it results in evolution of nitrogen on anode what eliminates the risk of hydrogen explosion (the redox potential of water oxidation to oxygen is $E^o = 1.23$ V *vs.* RHE).

It is worth mentioning that in addition to ammonia, other nitrogen compounds, namely, hydrazine and urea are also the subject of the research, though ammonia is the least investigated out of the three. The disadvantages of using ammonia are its low solubility in water and its gaseous state. However, ammonia as a sacrificial agent has many advantages. The mass fraction of hydrogen in ammonia is 17.6%, which is higher than that in hydrazine (12.5%) and urea (6.6%). Ammonia oxidation does not emit CO_2 like urea and is a safer compound to handle than hydrazine. However, electrochemically dehydrogenated N atoms are easily further oxidized to NO_x, instead of getting dimerized to N_2, especially at high overpotentials. Both urea and hydrazine are obtained from ammonia, so it is economically advantageous to use ammonia for the assisted water electrolysis. In addition, the importance of the ammonia electrooxidation study can be extended for the development of

* Corresponding author.
E-mail addresses: justyna.luczak@pg.edu.pl (J. Łuczak), marek.lieder@pg.edu.pl (M. Lieder).

https://doi.org/10.1016/j.cis.2023.102963
Received in revised form 5 July 2023;
Available online 16 July 2023

ammonia fuel cells [2], sensors [3] and wastewater treatment [4].

The ammonia oxidation process attracted interest as early as the 1960s' [5]. It was established that water electrolysis on Pt in ammonia aqueous solutions proceeds as follows (Eq. 1–3):

$$\text{Anode}: 2NH_3 + 6OH^- \rightarrow N_2 + 6H_2O + 6e^- \quad (1)$$

$$\text{Cathode}: 6H_2O + 6e^- \rightarrow 3H_2 + 6OH^- \quad (2)$$

$$\text{Overall reaction}: 2NH_3 \rightarrow N_2 + 3H_2 \quad (3)$$

As the reactions show, water used in the cathodic process comes from the anodic oxidation of ammonia, which is the indirect source of hydrogen evolving on the cathode.

The exact mechanism of ammonia oxidation is not yet recognized. However, based on the results of studies conducted for Pt, as the most active electrocatalyst of AOR, it was assumed that this process can follow two mechanisms (Fig. 1). First one, proposed by Oswin and Salomon [6] (O—S mechanism), proceeds by successive dehydrogenation of NH_3 to adsorbed atomic nitrogen (N_{ads}), followed by its dimerization to N_2. Later studies showed that AOR proceeding according to this mechanism leads to poisoning of the Pt surface by N_{ads} [7]. The mechanism proposed somewhat later by Gerischer and Mauerer [8] (G-M mechanism) takes into account the coupling of the dehydrogenated $NH_{x,ads}$ species into $NH_{x,ads}$-$NH_{x,ads}$ ($1 \leq \Sigma H \leq 4$), followed by their further dehydrogenation to N_2. In both mechanisms the OH^- ions taking part in the reaction come directly from the solution (without preceding adsorption). These mechanisms were confirmed experimentally by spectroscopic technics [9] as well as DFT calculations [10].

Selected limitations of the practical application of Pt as the electrocatalyst for AOR are as follows: *(i)* susceptibility to poisoning due to formation of N_{ads} or other oxygenated nitrogen species at potentials >0.65 V *vs.* RHE [7]; *(ii)* high overpotential (*ca.* 0.5–0.6 V [11]) which may result in strong polarization, therefore, part of the electricity is used for water oxidation, thus the evolution of oxygen; *(iii)* poor selectivity of the catalyst which leads to NO_x formation instead of N_2 at potentials higher than 0.8 V *vs.* RHE [11].

The above-described characteristics have given rise to search for other electrocatalysts based on non-noble metals in particular. From the very beginning of the research on AOR [5], Ni was considered as a possible alternative to Pt due to its electrochemical stability in alkaline medium, which is a prerequisite for the presence of ammonia in nonionic form (pKa = 9.25). The good electrochemical properties of nickel, in particular its hydro(oxides), as a single non-metal electrocatalyst are attributed to its close to unity e_g occupancy of the 3d electron in Ni^{3+} (t_{2g6} e_{g1}) ions. Therefore, Ni-based species with a valence state of 3+ have been used in NiCd or NiH batteries [12] and also reported to be very good material for OER [13], though their stability was not as high as expected. Accordingly, nickel (metallic), its alloys, oxides, hydroxides, and some composite materials have been considered as promising electrocatalysts for ammonia oxidation reaction. The up-to-date literature includes reviews on: *(i)* the AOR mechanisms [14,15], *(ii)* electrocatalysts for AOR with special emphasis on noble metals [15–18], *(iii)* non-noble metals for AOR [17] *(iv)* the use of AOR in fuel cells [19–21]. In our opinion, those reviews do not address thoroughly the significance of nickel oxyhydroxides in the mechanism of AOR.

In the presented work, the electroactivity of Ni is analyzed and discussed taking into account its all oxidation states. The analyzed data are compared to properties of the Pt catalysts as a benchmark. We highlight those composite/alloy materials for which Ni is confirmed to be the electroactive center of AOR, while the other components modify its properties. We focus on the AOR mechanism, the catalysts activity, selectivity, durability, and efficiency. The properties described are of particular relevance to assisted water electrolysis, electricity generation in fuel cells, and removal of ammonia from wastewaters. We also identify the main challenges for future research and the research problems to be solved so that the industrial use of ammonia as a hydrogen carrier can be expanded.

2. Nickel based electrocatalyst for ammonia oxidation

In this chapter, the possibility of ammonia oxidation on nickel of various oxidation states confirmed by theoretical calculations and experimental works are presented.

2.1. Nickel(0)

The standard enthalpy of solution of gaseous ammonia in water to form the non-ionized solute was found to be −35.3 kJ/mol (−0.37 eV) at 298 K [22], whereas the standard enthalpy of adsorption of ammonia on Ni surface from gaseous phase ranges from −63 to −100 kJ/mol (from −0.65 to −1.03 eV) [23,24]. Thus, the adsorption of ammonia on the Ni surface is energetically favorable. Moreover, theoretical calculations indicate that on Ni(111) the adsorption energy increases in the following sequence: N_2 (−0.42 eV) < NH_3 (−0.72 eV) < NH_2 (−2.72 eV) < NH (−4.52 eV) < N (−5.3 eV). Despite the increase in the adsorption energy, the length of the N—H bonds practically does not change, in other words, their energy does not decrease [25]. It is worth noting that the stability of the mentioned individuals on the Ni surface is close to that on the other catalytic surfaces, *e.g.* Pt(111) [26] and Rh(111) [27].

From thermochemical calculations [10,28] (Table 1), the onset potentials of AOR at Ni(111) were estimated to 0.56 V (NH_{ads} ➔ N_{ads}) and 0.33 V ($HNNH_{2,ads}$➔ $HNNH_{ads}$) for the O—S and the G-M mechanisms, respectively, whereas at Ni(100) was estimated to 0.25 V (NH_{ads} ➔ N_{ads}) and 0.06 V (NNH_{ads} ➔ N_2) for the O—S and the G-M mechanisms,

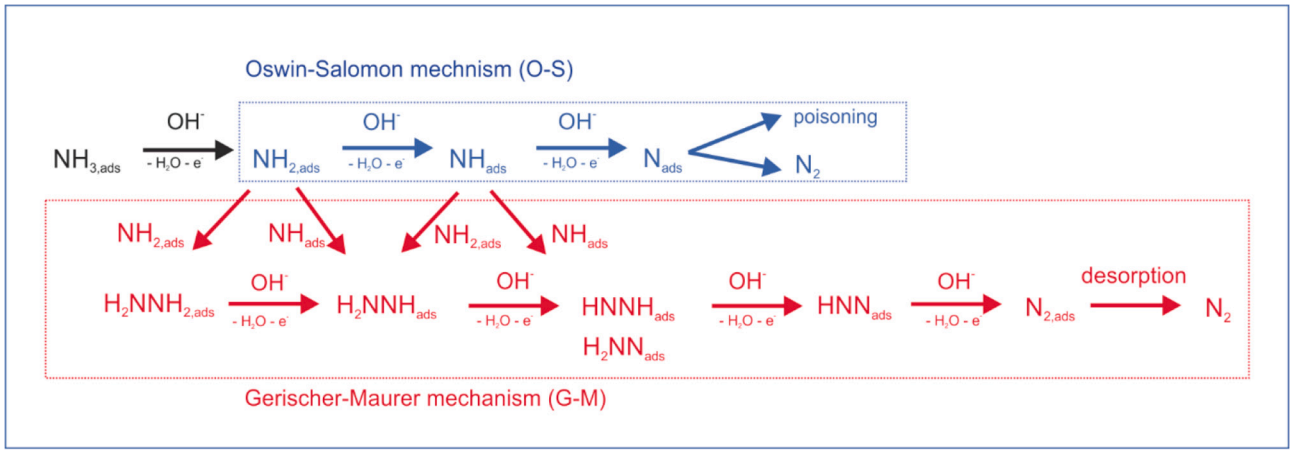

Fig. 1. The mechanisms of ammonia oxidation reaction to nitrogen.

Table 1
Selected thermodynamical, kinetical parameters and limiting steps of ammonia oxidation on platinum and nickel electrodes obtained by computational calculations.

	Onset potentials[i]		Activation energy[ii]		Gibbs free energy change		Preferential energy pathway
	Value [V vs. RHE]	Step	Value [eV]	Coupling step	Value	Coupling step	
Ni(100)	0.06 [28] 0.25 [28]	$NNH_{2,ads}$ ➔ NHH_{ads} NH_{ads} ➔ N_{ads}	2.28 [28] 3.30 [28]	N_{ads}-NH_{2ads} N_{ads}-N_{ads}			N_{ads}-NH_{2ads} at 0.4 V [28]
Ni(111)	0.33 [10] 0.56 [10]	$HNNH_{2,ads}$➔ $HNNH_{ads}$ NH_{ads} ➔ N_{ads}	–	–	–	–	–
β-$Ni(OH)_2$	1.52 [34]1.58 [34]	NH_{ads}-NH_{ads} N_{ads}-N_{ads}	–	–			NH_{ads}-NH_{ads} [34]
Pt(100) G-M	0.29 [28] >0.50* [11]	$HNNH_{ads}$ ➔ NNH_{ads} $NH_{x,ads}$ formation	0.56 [28] ~0 [11]	N_{ads}-NH_{ads} N_{ads}-NH_{ads}	~ − 0.7 eV	N_{ads}-NH_{ads} [31]	N_{ads}-N_{ads} at 0.4 V [28]
Pt(100) O-S	0.87 [28]	$NH_{2,ads}$➔ NH_{ads}	0.53 [28] ~0 [11] 0.1 [31]	N_{ads}-N_{ads} N_{ads}-N_{ads} N_{ads}-N_{ads}	−1.5 eV	N_{ads}-N_{ads} [31]	N_{ads}-N_{ads} at 0.9 V [28] NH_{ads}-NH_{ads} at 0.6 V [28]
Pt(111)	0.28 [10] 0.52 [10]	$H_2NNH_{2,ads}$➔ $HNNH_{2,ads}$ NH_{ads} ➔ N_{ads}	1.07 eV 2.24 eV	$NH_{2,ads}$-$NH_{2,ads}$ [10] N_{ads}-N_{ads} [10]			NH_{2ads}-NH_{2ads} at 0.4 V [10]

[i] other authors call this parameter limiting potential [34] or formation potential [11],
[ii] activation energy of non-farradaic steps of AOR, for the G-M mechanism, values are given for the step with the lowest activation energy,
* experimental value,

respectively. These data indicate that Ni may be a good electrocatalysts for AOR and Ni(100) shows lower onset potentials for both mechanisms. For comparison, the onset potentials at Pt(111) were calculated to be 0.52 V (NH_{ads} ➔ N_{ads}) and 0.28 V ($H_2NNH_{2,ads}$➔ $HNNH_{2,ads}$) for the O—S and the G-M mechanisms, respectively, whereas the relevant potentials at Pt(100) are 0.87 V ($NH_{2,ads}$➔ NH_{ads}) and 0.29 V ($HNNH_{ads}$ ➔ NNH_{ads}) for the O—S and the G-M mechanisms, respectively. For the (111) plane, the differences in these characteristic potentials between Ni and Pt are minimal, although for the G-M mechanism different dehydrogenation reactions were considered for their evaluation. In the case of (100) facet, the onset potentials calculated at Ni(0) was found to be lower than that at Pt(0), thus may suggest that Ni(0) could be a more active catalyst than Pt(0) for AOR. Although these characteristic potentials at Ni are favorable in comparison to Pt, for the G-M mechanism the slow kinetics of N—N formation was pointed to limit the overall reaction rate (kinetic aspect) [10].

As far as non-faradic steps are considered their energy barriers for both mechanisms were calculated by Elnabawy et al. [28] as shown in Table 1. For the O—S mechanism, this is the dimerization of N_{ads}, while for the G-M one the dimerization of NH_x (where $x = 0 \div 2$) to hydrazine or other intermediate species. In the case of Pt(100), the calculated activation energy of N—N formation resulting from N_{ads} dimerization is 0.53 eV, while for the G-M mechanism the activation energy of hydrazine formation was estimated to be 2.32 eV. Thus, the authors concluded that Pt(100) should not be poisoned by N_{ads}, but as we show further in the article, the experiments to date do not confirm this [11]. High energy barrier of hydrazine formation was also confirmed by Li et al. [29]. For Pt(111), on the other hand, the relevant calculated activation energy is 2.24 eV for N_{ads} coupling, whereas 2.69 eV for NH_{ads} dimerization (the NH_2-$NH_{2,ads}$ barrier formation is 1.07 eV) [28]. Thus, the energy barrier for the $NH_{2,ads}$ dimerization is much higher for Pt(100) than for Pt(111). However, Wallace et al., based on the DFT calculations, concluded that at high coverage of $NH_{2,ads}$ their dimerization barrier at Pt(100) becomes much lower [30].

Meanwhile, Katsounaros et al. [11] and Elanbawy et al. [28] showed that, the lowest energy barrier are for the N-N_{ads} and N-NH_{ads} formation at Pt(100). Nevertheless, the last step of NH dehydrogenation is slow, that is why the authors postulated that the most feasible pathway is the NH_{ads} coupling. For comparison, the lowest energy barrier for Pt(111) was shown for $NH_{2,ads}$ dimerization [28].

The calculation results (Table 1) show that Pt(100) should not undergo poisoning by N_{ads} thank to the low energy barrier of the N_{ads} dimerization. However, the experimental results [11], show that Pt (100) suffers from poisoning when its potential exceeds 0.63 V. In this regard, Pillai et al. [31] and Katsounaros et al. [11] proposed that it is not nitrogen that poisons the surface of Pt, but the intermediates of ammonia oxidation (namely $NH_{x,ads}$ or NO_{ads}) or hydroxide/oxide species such as OH_{ads}/O_{ads}. Similarly, Matsui et al. [9] by using ATR-IR technique revealed the presence of NO species on the Pt electrode surface is probably responsible for poisoning platinum at higher potentials. The conversion of NH_3 to NH_x upon reaction with adsorbed oxygen-containing species and formation of various reaction products (NO, N_2O, N_2, and H_2O) was also confirmed by DFT calculations by Novell-Leruth et al. [32]. The potentiodynamic measurements performed by Koper et al. revealed that at Pt(111), in the potential region more positive than 0.65 V, AOR is strongly inhibited (Pt surface poisoned by N_{ads}) due to the very high activation energy of the N_{ads} dimerization step [7,33]. To our best knowledge there is no experimental evidence for the existence of species other than N_{ads} on the surface of Pt(111).

For the O—S mechanism, the calculated activation energy of N—N formation at Ni(100) is 3.30 eV (Table 1). This value is higher than the one for the other non-faradaic nitrogen coupling steps assumed for the G-M mechanism. The lowest energy barrier is 2.28 eV for N_{ads}-NH_{2ads} step [28]. For the Ni(111) surface, the activation energy data are not available according to our knowledge. We could expect the Ni surface to be poisoned in the same way as Pt(111), though at much higher potentials, as first-principle studies show, Ni binds $NH_{x,ads}$ and NH_x-$NH_{x,ads}$ even more strongly than Pt (besides NH_2-$NH_{2,ads}$) [10]. Thus, throughout the entire range of potentials, Ni activity should be relatively low.

Summarizing, the higher value of the onset potential and the higher activation energy barrier of N_{ads} dimerization [28] implies that the G-M mechanism will prevail on the Ni(100) facet. This assumption has yet to be experimentally verified, however, it is difficult because the Ni surface passivates (nickel oxides are formed) [35]. Passivation of Ni begins at pH higher than 5.5 (as DTF calculations show), however, according to the experimental results $Ni(OH)_2$ is stable above pH 9 [36]. Therefore, theoretically, passivation of Ni surfaces could be avoided by using for AOR the solution with pH lower than 8. Unfortunately, at pH lower than 9.25 (pKa), ammonia is present in solution mainly as NH_4^+ ions, with the consequence that the concentration of free NH_3 at the electrode surface to be too low for effective oxidation rate [37].

2.2. Nickel(II)

Nickel potential−pH (Pourbaix) diagram improved by Huang et al. [36] using state-of the-art first-principles calculations in combination with modern electrochemical measurements (electrochemical impedance spectroscopy, EIS and surface enhanced Raman spectroscopy, SERS) is shown in Fig. 2. NiO and $Ni(OH)_2$ are stable at pH ≥ 5.0 and 6.1

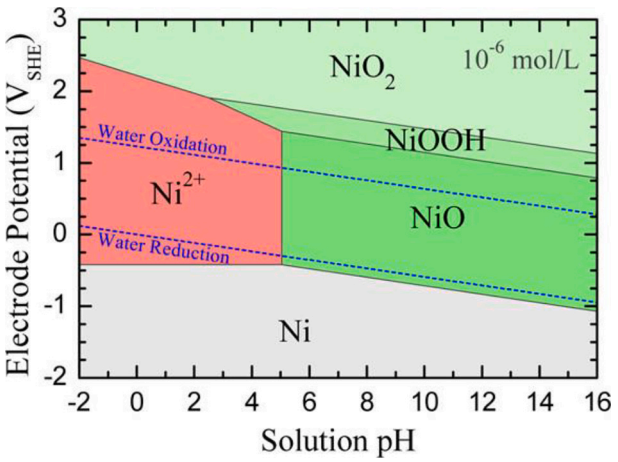

Fig. 2. Potential-pH diagram of nickel species at 298.15 K, 1.0 bar [36].

(not shown), respectively, below which they dissolve.

Ni electrode immersed in alkaline solutions becomes spontaneously covered with thin layer of NiO/$Ni(OH)_2$ (eqs. 4–5) [38], which thickness can be further increased by anodic polarization:

$$Ni + 2OH^- \rightarrow Ni(OH)_2 + 2e^- \quad (4)$$

$$Ni + 2OH^- \rightarrow NiO + H_2O + 2e^- \quad (5)$$

According to Smith et al. [39], who used *in situ* differential reflectometry technique, a film composed of $Ni(OH)_2$ accompanied by NiO grows on the electrode surface at intermediate potentials (polarization in de-aerated solution of 1 M Na_2SO_4 0.88 V *vs.* RHE). These observations were confirmed by Zhang et al. [40], who revealed a bilayer structure of the surface film consisting of the inner NiO layer and the outer $Ni(OH)_2$ layer by the X-ray photoelectron spectroscopy (XPS) analysis (polarization at 1.23 V *vs.* RHE, pH 9.2). The SERS spectra, in turn, indicated the formation of an amorphous $Ni(OH)_2$ film without NiO (at 1.33 V *vs.* RHE, pH 8.4) [41].

$Ni(OH)_2$ can be synthetized as a stack of layers intercalated with water molecules and electrolyte ions. There are two known crystallographic structures: α-$Ni(OH)_2 \bullet xH_2O$, $0.41 < x < 0.47$ and β-$Ni(OH)_2 \bullet xH_2O$, $0.1 < x < 0.4$. The intercalated water molecules hold together Ni

Table 2
Selected redox potentials of nickel, nitrogen and their derivatives [1]

No.	Half-cell reaction	E°, V vs. RHE
	$Ni(OH)_2 + 2e^- \rightarrow Ni + 2OH^-$	0.106
	$NiO + H_2O + 2e^- \rightarrow Ni + 2OH^-$	0.116
	$NiOOH + H_2O + e^- \rightarrow Ni(OH)_2 + OH^-$	1.300
	$2CuO + H_2O + 2e^- \rightarrow Cu_2O + 2OH^-$	0.606
	$CuO + H_2O + 2e^- \rightarrow Cu + 2OH^-$	0.536
	$Cu_2O + H_2O + 2e^- \rightarrow 2Cu + 2OH^-$	0.461
	$NH_2OH + H_2O + 2e^- \rightarrow NH_{3(aq)} + 2OH^-$	1.246
	$0.5\ N_2 + 3H_2O + 3e^- \rightarrow NH_{3(g)} + 3OH^-$	−0.057
	$0.5\ N_2 + 3H_2O + 3e^- \rightarrow NH_{3(aq)} + 3OH^-$	−0.092
	$0.5N_2O + 3.5H_2O + 4e^- \rightarrow NH_{3(aq)} + 4OH^-$	0.510
	$NO_{(g)} + 4H_2O + 5e^- \rightarrow NH_{3(aq)} + 5OH^-$	0.727
	$NO_2^- + 5H_2O + 6e^- \rightarrow NH_{3(aq)} + 7OH^-$	0.806
	$NO_3^- + 6H_2O + 8e^- \rightarrow NH_{3(aq)} + 9OH^-$	0.875*
	$2NO + 2H_2O + 4e^- \rightarrow N_{2(g)} + 4OH^-$	1.678
	$2NO_2^- + 4H_2O + 6e^- \rightarrow N_{2(g)} + 8OH^-$	1.520
	$2NO_3^- + 6H_2O + 10e^- \rightarrow N_{2(g)} + 12OH^-$	1.246

* approximate value, more precise data are missing [1].

$(OH)_2$ layers and have freedom to rotate and translate between the planes. The possible types of structural disorders involve not only variable hydration but also incorporation of foreign ions, stacking faults and other crystal defects [35]. α-$Ni(OH)_2$ has a large charge capacity (482 mAh/g), low charge and high discharge voltages and large volume expansion in comparison with β-$Ni(OH)_2$ [35]. Moreover, electrical conductivity of α-$Ni(OH)_2$ is higher due to larger water content [42]. Concentrated alkaline solution (so called "aging") causes the removal of intercalated water from α-$Ni(OH)_2$ and its recrystallization to the β-Ni $(OH)_2$ form, in which the interlayer distance is much shorter. The interlayer water in α-$Ni(OH)_2$ is removed at $T \approx 240$–300 °C, whereas dehydration of β-$Ni(OH)_2$ proceeds between 160 °C < *T* < 525 °C and begins with expulsion of the intercalated water and ends up with decomposition of $Ni(OH)_2$ to NiO [35].

There are no experimental results confirming catalytic activity of Ni $(OH)_2$ for ammonia electrooxidation reaction prior to its conversion to NiOOH (see subchapter 3. *Nickel(III)*). An attempt to theoretically analyze the mechanism of AOR on β-$Ni(OH)_2$ was undertaken by Choueiri et al. [34]. The authors postulated that the evolution of N_2 on the β-$Ni(OH)_2$ surface undergoes through NH-NH_{ads} coupling as the lowest energy path. The calculated limiting potentials for N_2 formation are 1.52 and 1.58 V *vs.* RHE for NH_{ads}-NH_{ads} and N_{ads}-N_{ads} coupling, respectively. These results cannot be confirmed experimentally, since the transformation of $Ni(OH)_2$ to NiOOH is observed in this potential range.

2.3. Nickel(III)

Near the oxygen evolution potential, $Ni(OH)_2$ is reversibly transformed into higher-value oxide:

$$Ni(OH)_2 + OH^- \rightarrow NiOOH + H_2O + e^- \quad (6)$$

According to the Bode cycle [43], α-$Ni(OH)_2$ may undergo transformation to γ-NiOOH, whereas β-$Ni(OH)_2$ to β-NiOOH (two distinct redox transitions: β/β and α/γ), as shown in Fig. 3. α-$Ni(OH)_2$ can be converted at potential about 40 mV lower than the corresponding β-Ni $(OH)_2$ form. α-$Ni(OH)_2$ can be fully oxidized to γ-NiOOH prior to the onset of OER [44]. Multiple potential cycling of the nickel hydroxide electrode (electrochemical oxidation by overcharging to 20%) results in an increase in electrical conductivity from 10^{-17} S/cm to 10^{-5} S/cm at 298 K, indicating change from insulating $Ni(OH)_2$ to a semiconducting NiOOH [42]. The phase transition between $Ni(OH)_{2(s)}$ and $NiOOH_{(s)}$ was confirmed by Raman spectrometry [45] and XPS [46].

It is known that α-$Ni(OH)_2$ is unstable in alkaline solutions since it undergoes irreversibly dehydration to the β-$Ni(OH)_2$ form. Therefore, some authors challenge the Bode cycle suggesting that during electrochemical experiments α-$Ni(OH)_2$ is not directly oxidized to γ-NiOOH because its conversion to β-$Ni(OH)_2$ can not be avoided. The proposed scheme of the reactions is as follows [47] α-$Ni(OH)_2$ ➔ β-$Ni(OH)_2$ ➔ β-NiOOH.

β-NiOOH has a low theoretical capacity and if overcharged it transforms to γ-NiOOH (more disordered form), with simultaneous deterioration of electric contact with a current collector. Although β-NiOOH and γ-NiOOH have similar structures, the latter has the higher oxidation state (3.55–3.7) than β-NiOOH (3.0). Thus, this conversion leads to unbalanced positive charge, which drives anions from the bulk solution into the interlayer space increasing the distance between the layers from 4.8 Å in β-NiOOH to 7 Å in γ-NiOOH [35,48]. This should be associated with the larger charge capacity [48,49]. The average oxidation state of Ni in each phase and the interlayer distances are shown in Fig. 3.

Considering the aforementioned electrochemical properties of α-Ni $(OH)_2$, it would be beneficial to produce and stabilize this structure, to let its direct conversion to γ-NiOOH. In this regard, NiOOH is formed directly on the electrode by electrochemical oxidation of nickel. In another approach, chemical syntheses of $Ni(OH)_2$ are employed (*e.g.* sol-gel) followed by deposition of the product onto the conductive support

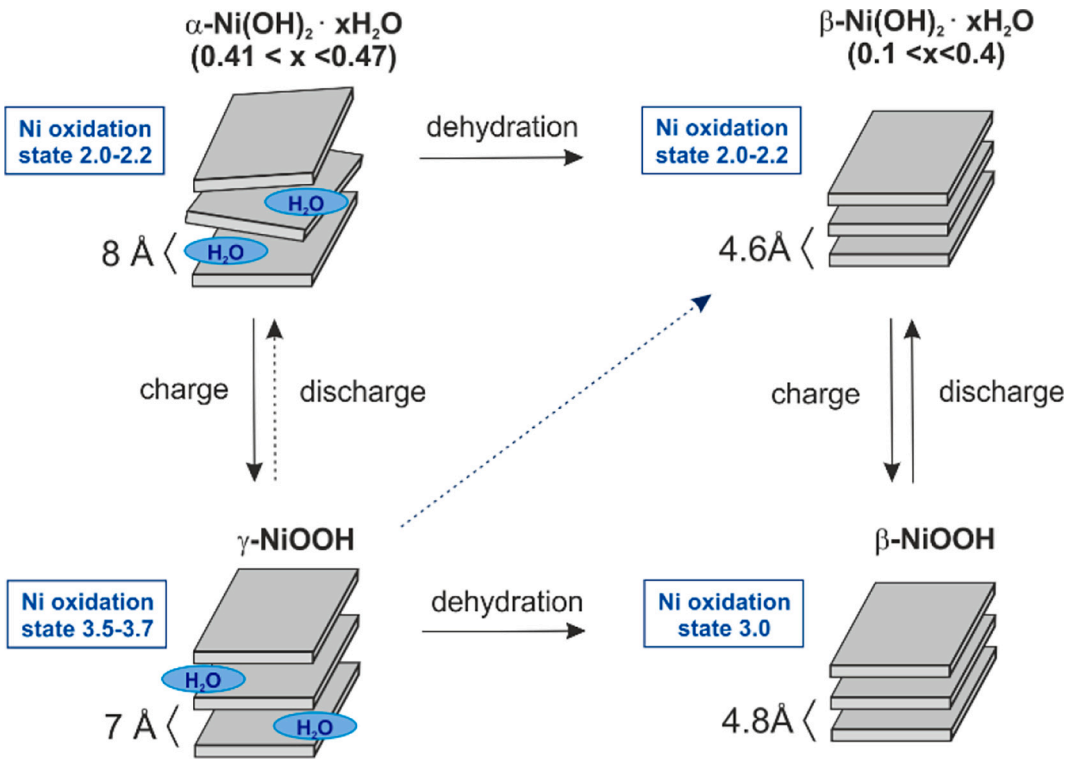

Fig. 3. *Diagram of Bode cycle (adapted from* [45,51]*).*

(electrode) [50].

β-NiOOH is most often reduced to β-$Ni(OH)_2$, while γ-NiOOH to the α phase. γ-NiOOH may also convert to β-$Ni(OH)_2$, but the process is less likely because it requires internal reconstruction including water expelling. It is worth noting that reduction of 1 mol γ-NiOOH involves ~1.6 mol of electrons.

As shown earlier, theoretical studies do not exclude catalytic activity of Ni(0) and $Ni(OH)_2$ towards AOR, however, numerous experimental results indicate that during polarization Ni(0) and $Ni(OH)_2$ undergo chemical reconstruction into NiOOH (eq. 7). The surface species after this reconstruction (E = ~1.3 V *vs* RHE) would serve as real active sites. Thus, the AOR begins at a very high overpotential ($E^o = -0.097$ *vs* RHE). As shown in the eq. (7), a proton and electron are transferred in a single-coupled step leading to indirect reduction of the Ni^{3+} to Ni^{2+} [52,53]

$$\overset{H^+ + e^-}{\frown}\quad NiOOH + NH_{3,ads} \rightarrow Ni(OH)_2 + NH_{2,ads} \tag{7}$$

According to some authors [34], the proton and electron transfer are decoupled (eq. 8). Proton goes to the solution whereas electron is transferred to the electrode without changing the oxidation state of Ni^{3+}.

$$\overset{H^+}{\frown}\quad OH^-_{aq} + NH_{3,ads} \rightarrow H_2O_{aq} + NH_{2,ads} + e \tag{8}$$

On the other hand, some studies have shown the presence of OH_{ads} on the surface of Pt or Ni (hydroxyl adsorption energy on Ni(100) is −349.03 kJ/mol (3.62 eV) [54], and Ni(111) is −315.5 (3.27 eV)kJ/mol and is higher than that on Pt(111) -246.7 kJ/mol (2.56 eV) [54]). This allows us to presume that during AOR the surface of these metals is simultaneously covered by OH_{ads} and $NH_{x,ads}$. Theoretically, the adsorbed OH_{ads} could also enable the $NH_{x,ads}$ dehydrogenation (eq. 9) since the energy of O—H bonding (463 kJ/mol; 4.8 eV) is greater than the energy of N—H bonding (391 kJ/mol; 4.1 eV).

$$\overset{H^+ + e^-}{\frown}\quad OH_{ads} + NH_{3,ads} \rightarrow H_2O_{ads} + NH_{2,ads} \tag{9}$$

Nevertheless, the role of OH_{ads} in the dehydrogenation of NH_3 at Ni has not been resolved yet. Though, a key role of OH_{ads} was established for example in the dehydrogenation of $NH_{3,\ g}$ at Au(111) [55] or the dehydrogenation reaction of hydrazine at Ni(111) [56]. Moreover, the formation of NH_{ads} becomes thermodynamically unfavorable at Pt(100) unless OH_{ads} is adsorbed. Coverage of the surface by OH_{ads} shifts the formation potential of NH_{ads} from 0.9 V to *ca.* 0.69 V *vs.* RHE [29]. Coadsorption of NH_3 and OH^- was theoretically investigated by Zhang et al. [57] for AOR on NiCu-FeOOH catalysts. The estimated adsorption free energies of OH^- were as follows: −123.5 kJ/mol (−1.28 eV) on FeOOH and 110.0÷136.0 kJ/mol (1.14÷1.41 eV) on metal sites in NiCu-FeOOH. After the initial coadsorption of NH_3 and OH^-, the dehydrogenation of NH_3 took place.

The catalytic activity of β-NiOOH could be also moderated by the presence of hydroxide and oxygen vacancies as was recently reported by Choueiri et al. [58]. The DFT calculations point to the G-M mechanism as more thermodynamically favorable. The lowest energy pathway towards N_2 proceeds through NH—NH coupling for NiOOH with oxygen vacancies (0.97 V *vs.* RHE) whereas surfaces with hydroxide vacancies favors NH_2—NH_2 coupling (1.12 V *vs.* RHE). In comparison, for the N_{ads} dimerization the lowest energy for NiOOH with oxygen vacancies occurs at 1.76 V *vs.* RHE and with hydroxide vacancies at 2.17 V *vs.* RHE [58].

One of the earliest successful electrooxidation of NH_3 at the Ni electrode was published by Kapalka et al. in 2010 [37]. They carried out multiple polarizations of clean solid Ni electrode (200 scans) in the potential range of −0.18 V and 1.87 V *vs.* RHE thereby oxidizing the Ni surface, initially to $Ni(OH)_2$ and then to NiOOH. The current measured in the CV experiments was responsive to changes in the concentration of ammonia in the solution. The solutions used for these experiments were composed of NH_4ClO_4 in 1 M $NaClO_4$ + NaOH at pH 9 and 25 °C. These findings were later on extended to Ni foam (NF) and elaborated by Shih et al. [59]. The CV studies revealed two reversible peaks, first one at

onset potential of ~1.40 V *vs.* RHE attributed to transformation of α-Ni $(OH)_2$ to γ-NiOOH and the second one at 1.64 V *vs.* RHE assigned to the β-$Ni(OH)_2$ to β-NiOOH conversion. The experiments were carried out in solutions composed of 0.001–0.03 M $(NH_4)_2SO_4$, 0.01 M Na_2SO_4, at pH 11 and 25 °C. Another approach was adopted by Almomani et al. [60], who synthesized *ex-situ* NiO and NiO-TiO_2 nanocatalysts, which then were mixed with carbon black to obtain conducting composite electrodes. The cyclic voltammetry measurements were done at pH 9 in a 0.2 M NH_4^+, 0.1 $NaNO_3$ solution. The activity of NiO and NiO-TiO_2 towards AOR was achieved by their conversion to NiOOH which existence was confirmed by the XPS measurements. Gonzalez-Reyna et al. [61] studied AOR using working electrodes composed of Ni nanoparticles deposited on carbon nanotubes (CNT—Ni) and carbon nanospheres (CNS-Ni) in a solution composed of 200–600 ppm $(NH_4)_2SO_4$ in 0.01 M K_2SO_4 + KOH at pH 11. Before the ammonia oxidation experiments, the electrodes were polarized to form $Ni(OH)_2$. The authors also assigned the AOR to the conversion of $Ni(OH)_2$ to NiOOH. Hydrophilization of the surface of the carbon nanostructures contributed to increasing the specific surface area on which the Ni catalyst was deposited. Higher catalytic activity was preserved for CNS-Ni, for which the rate of ammonia decomposition was 3.63 ppm/h. Medvedev et al. [50] analyzed the performance of the $Ni(OH)_2$/NF electrode in 0.025–0.2 M NH_3, 0.1 M Na_2SO_4 and NaOH solutions at pH 9÷14. The reported onset potential of AOR was 1.4 V, and the presence of N_2 was confirmed to decrease in the potentials range of 1.6–2.2 V. On the contrary, Huang et al. [62], who synthetized $Ni(OH)_2$-Cu_2O@CuO on NF (Fig. 4), observed mainly N_2 evolution and minute volume of O_2 (1.54 V *vs.* RHE). The authors do not state whether this unusually high selectivity of the reaction is to be attributed to the presence of Cu. However, Cu_2O@CuO enhances catalytic activity of the $Ni(OH)_2$/NiOOH redox couple. A much higher current density (~60 mA/cm^2 at 1.59 V *vs.* RHE) was obtained in a solution composed of 1 M NH_3 and 1 M KOH (Fig. 5). The activity of the catalytic materials deposited on NF increased in the following order: $Ni(OH)_2$-Cu_2O@CuO > Cu_2O nanowires > > $Ni(OH)_2$, however, the authors do not consider Cu compounds as the redox centers.

Xu et al. [63] synthetized hierarchical mixed NiCu layered hydroxides (LHs) nanowires on carbon fiber cloth. It has been observed that Cu causes an enlargement of NiCu hydroxides' surface area and thus the catalytic activity (Fig. 6). On the other hand, Co, Fe, Zn, Mn, or Cr cause deactivation of Ni. Jiang et al. [64] analyzed nanocomposites of Cu

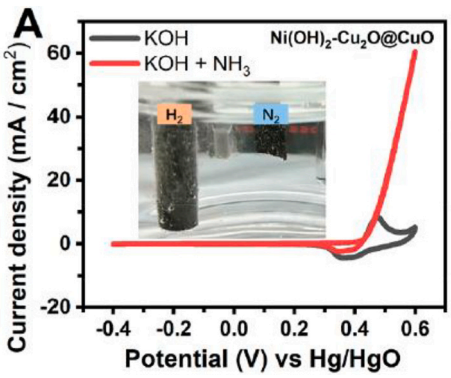

Fig. 5. Cyclic voltammetry of $Ni(OH)_2$-Cu_2O@CuO on the Ni foam performed in solution of 1 M KOH without and with 1 M NH_3 (potential range from 0.59 to 1.59 V vs. RHE) [62].

$(OH)_2$ nanoparticles homogeneously distributed in $Ni(OH)_2$. Presence of Cu hydroxide islands on the electrocatalyst surface lowered the onset potential of AOR from 1.52 V *vs.* RHE to 1.40 V (pH 13, 0.1 mol/dm^3 KOH and 0.5 mmol/dm^3 $(NH_4)_2SO_4$). Similar influence of Cu was reported by Song et al. [52], who co-deposited Ni and Cu on boron doped diamond (BDD) followed by their electrochemical oxidation of metals to hydroxides. Based on the theoretical calculations, the authors postulated that these metals stabilize the relative energies of the NH_x intermediates thus promoted the ammonia oxidation process.

Zhang's group used a method of manufacturing catalysts involving electrodeposition of metals followed by electrochemical tuning in alkaline solutions to reconfigure the surface (presumably turning metals into hydroxides). In [65] NiCu were deposited on NF, whereas in [66] NiCuCo doped by S were deposited on carbon paper. The CV experiments showed that the ammonia oxidation process begins at *ca.* 1.2–1.3 V for both NaOH and NaOH + NH_4Cl solutions observed as the increase of the current due to conversion of Ni^{2+} to Ni^{3+}. The value of these potentials is about 100–200 mV lower than the ones reported for the other Ni-based electrocatalysts ([59,64]). The authors did not discuss this observation. Both catalysts are active towards AOR as shows an increase of current densities to ~40 mA/cm^2 for NiCu- [65] and ~ 73 mA/cm^2 in case of NiCuCo/S-based catalysts [66] for identical parameters, *i.e.* ~1.55 V *vs.* RHE, 1 M NaOH +0.4 M NH_4Cl solutions. A

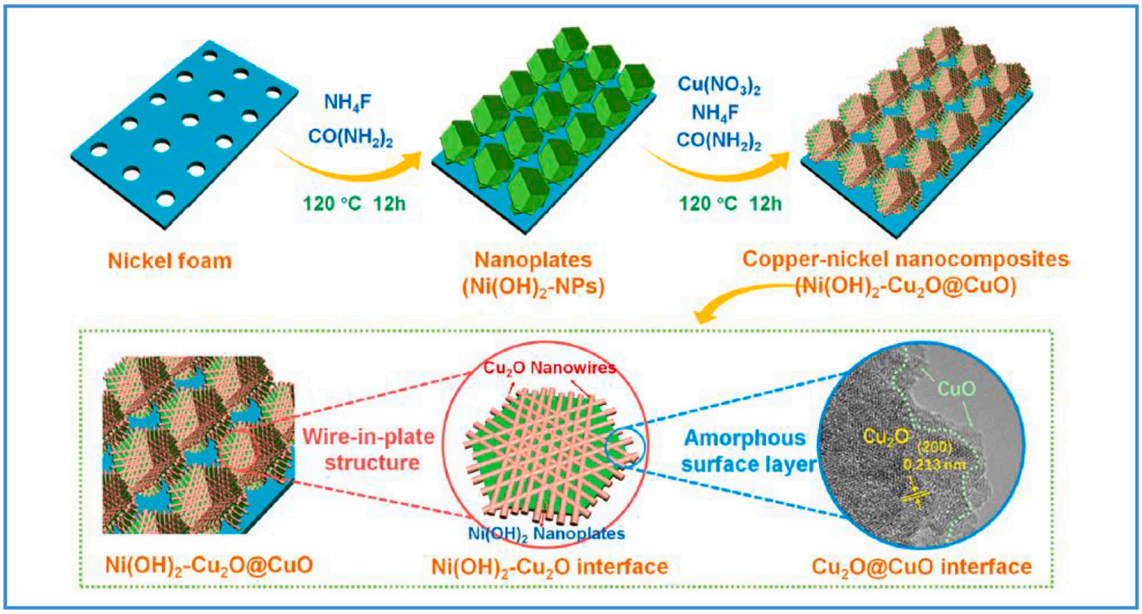

Fig. 4. The $Ni(OH)_2$-Cu_2O@CuO electrocatalyst deposited on nickel foam [62].

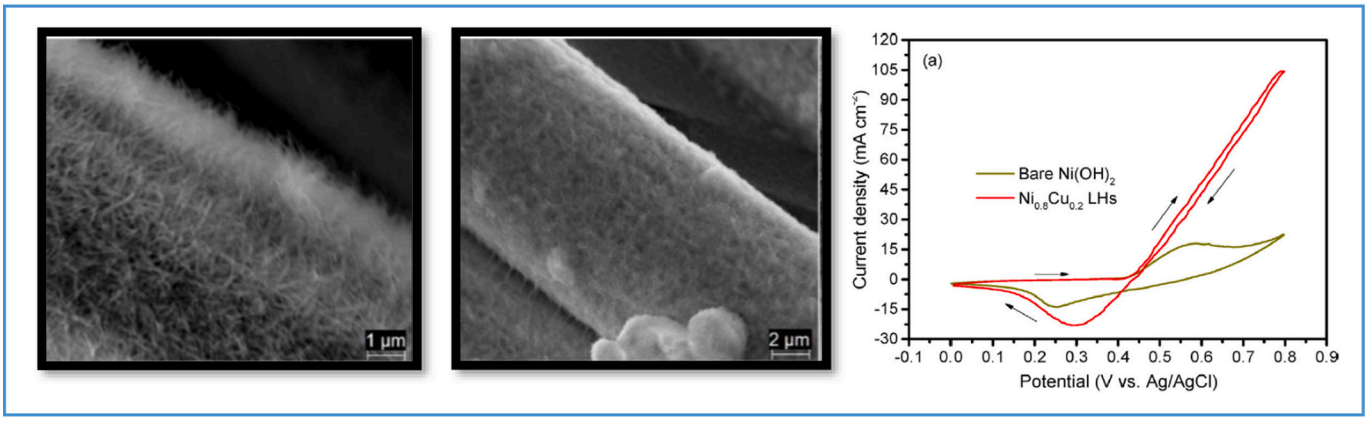

Fig. 6. SEM images of a) $Ni(OH)_2$ and b) $Ni_{0.8}Cu_{0.2}$ layered hydroxides (LHs) growing on carbon fibers; c) cyclic voltammetry of $Ni_{0.8}Cu_{0.2}$ and $Ni(OH)_2$ in solution composed of 0.5 M NaOH and 55 mM NH_4Cl at scan rate of 25 mV s^{-1} [63].

maximum current density of 90 mA/cm^2 at the potential of 1.53 V was obtained for 3 M NaOH +0.4 NH_4Cl solution [65] and 121 mA/cm^2 at 1.65 V for 3 M NaOH +0.2 NH_4Cl solution. The enhanced electrocatalytic activity of the NiCu-based catalyst was attributed to the 3D structure, whereas NiCuCo/S-based one to synergistic effect between active metals, thus improved their adsorption/desorption properties. Unfortunately, the authors did not compare the current values normalized against the effective catalyst surface area (ECSA). High current density (90 mA/cm^2 at ~1.55 V *vs.* RHE, 1 M KOH + 0.3 M NH_3) was also recorded by Latvyte et al. for a nickel-copper co-electrodeposited catalyst onto a nickel felt. A long-term experiment (50 h at 20 °C) performed at a current density of 100 mA/cm^2 (cell potential 1.69–1.78 V) showed the electrode maintained a stable AOR rate [67]. Tsai et al. [68] investigated the ammonia oxidation using Cu electrodeposited on NF. The XPS analysis revealed that NH_3 facilitates oxidation of Cu_2O to $Cu(OH)_2$, which according to the authors suggestion catalyzes the AOR alongside with NiOOH. The catalytic activity of Ni—Cu composites was also studied by Rahardjo et al. (Ni and NiCu oxides with Pt nanoparticles) [69], Zhang et al. (NiCu alloy on CNTs) [70] and (NiCu alloy nanoparticles covered with NiOOH and CuO on carbon paper) [71], and Zhu et al. (Ni—Cu hydroxides with Fe dopants) [72] and Hu et al. (N–NiZnCu LDH/reduced graphene oxide on Ni foam) [73].

The above-described reports show that addition of copper/copper oxides to Ni-based catalysts have promising effect on their performance, *e.g.*, higher activity. Nevertheless, the role of copper in the oxidation of NH_3 is still not clear and needs further studies. It is worth noting that the earlier DFT calculations [10] indicated NH_x binding energies on metallic Cu to be very weak, thus it should not be a good catalyst for the dehydrogenation of NH_3 to N_2. The analysis of the redox potentials shown in Table 2, also indicate that one can indeed hardly expect Cu moieties to be the charge transfer centers for the NH_3 oxidation. According to our knowledge, there are no theoretical predictions of the copper oxides' catalytic activity.

There are a few publications in which other Ni-based bimetallic materials have been analyzed for AOR, however, the results are not as promising as for Cu, so the number of reports is much lower. Although Xu et al., in the aforementioned paper [63], found out that Co hindered Ni activity, the other researchers reported opposite results [74,75]. Shih et al. [74] assumed that ammonia oxidation was mediated by bimetallic M(II)/(III) (M = Ni and Co) redox couple. Another studied bimetallic composite for AOR was AgNi obtained by electroplating metallic Ag nanoparticles on Ni [76]. The electrocatalytic AOR performed in the solution containing 3 mM NH_4^+ and 0.1 M Na_2SO_4, pH 11, was mediated by the redox series of Ag(II)/Ag(I) and Ni(III)/Ni(II). The effect of Pd content in Ni_xPd_{1-x} (where x = 0.98, 0.93 and 0.58) electrocatalysts was analyzed by Allagui et al. [77] for the solution composed of 0.2 M NH_4NO_3, 0.5 M $NaNO_3$ at pH 10.5. In this system, the active center of the NH_3 oxidation was also assign to the presence of NiOOH obtained by the electrolytic treatments of Ni. It was shown that increase in the Pd content decreases the size of the Ni nanoparticles from 50 to 100 nm to 5–20 nm. Nevertheless, the addition of Pd did not result in the increase of Ni activity (lower current density was measured). Other reported data indicate that palladium shows no activity towards ammonia oxidation (0.1 M $(NH_4)_2SO_4$ + 0.2 M NaOH) [78]. In the above discussion, we highlighted those materials for which Ni is confirmed to be the electroactive center of AOR, while the other components modify its properties. Therefore, we have not included studies devoted to Pt—Ni composites, since in these materials Pt is the electroactive center (AOR at ~0.55 V *vs.* RHE).

There have been only three papers published on Ni-based materials modified by nonmetals so far, *i.e.* P [79], S [66] and C,N [80] ([66,80] were described above). Wang *et al* [79]synthetized Ni_2P deposited onto NF by thermal decomposition of NaH_2PO_2 at 350 °C in Ar atmosphere. The authors claim that during polarization, Ni_2P is converted to Ni oxyhydroxides which were the real active sites for the ammonia oxidation.

The aforementioned studies on using Ni-based catalysts for AOR were focused firstly on ammonia assisted hydrogen electrocatalytic production [81] and secondly on electrochemical remediation of ammonia-containing wastewater [82].

2.4. Higher oxidation states of nitrogen

The ammonia oxidation may also lead to the creation of nitrites and nitrates, according to the following reactions (10,11):

$$NH_3 + 7OH^- \rightarrow NO_2^- + 5H_2O + 6e^- \quad (10)$$

$$NH_3 + 9OH^- \rightarrow NO_3^- + 6H_2O + 8e^- \quad (11)$$

Beside anionic products, the evolution of gaseous nitrogen oxides (N_2O, NO, NO_2) may also proceed. According to the nowadays research, in this process oxidation of intermediate $NH_{x,ads}$ species (x = 0÷2) occur [11,33,34,58], *e.g.*:

$$N_{ads} + 4OH^- \rightarrow NO_2^- + 2H_2O + 3e^- \quad (12)$$

$$NH_{ads} + 5OH^- \rightarrow NO_2^- + 3H_2O + 4e^- \quad (13)$$

$$NH_{2,ads} + 6OH^- \rightarrow NO_2^- + 4H_2O + 5e^- \quad (14)$$

via hydroxylation steps:

$$N_{ads} + OH_{ads} \rightarrow NOH_{ads} \quad (15)$$

$$NH_{ads} + OH_{ads} \rightarrow NHOH_{ads} \quad (16)$$

$$NH_{2,ads} + OH_{ads} \rightarrow NH_2OH_{ads} \quad (17)$$

The total dehydrogenation of NH_3 was postulated by Koper group [11,33] to proceed at Pt and by Choueiri et al. [34] at β-Ni(OH)$_2$. However, the latter group found later on that only NH_{ads} and $NH_{2,ads}$ were hydroxylated at β-NiOOH (with OH/ O vacancies) because the complete dehydrogenation of NH_3 was energetically very demanding [58]. Therefore, it seems that formation of nitrogen oxides derivatives undergoes without $NH_{x,ads}$ coupling (Fig. 7). Confirmation can be also provided by the fact that in the case of electrooxidation of hydrazine, nitrogen oxides have not been detected.

Though, the oxidation of N_2 involving its non-dissociative adsorption step prior to the charge transfer cannot be outright excluded (eq. 18 and 19) [83]:

$$0.5N_2 + 4OH^- \rightarrow NO_2^- + 2H_2O + 3e^- \quad (18)$$

$$N_2 + 2OH^- \rightarrow NO + H_2O + 2e^- \quad (19)$$

But the oxidation of NH_3 to NO and NO_2^-/NO_3^- begins at lower potentials (0.727 V and 0.806/0.876 V *vs.* RHE, respectively) than the one for relevant oxidation of N_2 (1.678 and 1.52 V/1.246 *vs.* RHE) as shown in Table 2. The oxidation potential of Ni^{2+} to Ni^{3+} is close to the oxidation potential of water which affects the efficiency of the ammonia oxidation process (oxygen release) and also may facilitate the formation of oxygenated compounds of nitrogen.

There are a couple of reports in which concentrations of various products of AOR were experimentally measured. Shih et al. [84] observed that ammonia oxidation to NO_3^- took place at potentials surpassing 1.54 V *vs.* RHE. Moreover, higher potential, and thus higher current density, resulted in more efficient NH_3 removal, more selective nitrate formation at the expense of nitrogen [59]. Increase in current density from 0.2 to 2.0 mA/cm^2 resulted in an increase of the NH_3 removal (from ~50% to 98.5%) along with the NO_3^- selectivity (from ~50% to ~60%) and the suppressed N_2 selectivity (from ~50% to ~38%) regardless of the initial NH_3 concentration (Fig. 8). Higher NH_3 concentration (from 50 to 450 mg/dm^3) favored N_2 selectivity (from 20 to 60%). By increasing temperature from 20 °C to 40 °C, a decrease of ammonia oxidation from 96 to 84%, and NO_3^- formation from 98% to 65% for efficiency and selectivity, respectively, was noticed (electrolyte 0.01 M Na_2SO_4, NH_3 = 50 ppm, pH 11, constant current density = 1.5 mA/cm^2). At the same time, the N_2 selectivity increased from 2% to 35%. The similar trend was induced by increasing pH of the solutions (~10% at pH 7.5 and ~ 50% at pH 12). Also, Medvedev et al. [50] analyzed effect of pH on the AOR selectivity, though, they observed opposite relation. At pH 11.3, in the potential range of 1.6–1.7 V, N_2 was the main product of the reaction (~50%). In a strongly alkaline environment (pH 13), already at a potential of 1.6 V, the evolution of O_2 was observed along with the relatively higher amount of NO_2^- at the expense of N_2. With the increased potential, the amount of N_2 released further decreased in favor of NO_3^-.

For co-deposited Ni and Cu hydroxides, potentials exceeding 1.48 V *vs.* RHE led to the formation of mainly NO_2^- (~82% ÷ 98%) as it was reported by Jiang et al. [64]. Selectivity of the N_2 production decreased from 100% at pH 8 to 62.8% at pH 12, simultaneously the rate of ammonia removal increased from 6.5% to 60% in 6 h as it was shown for the NiCu/BDD electrocatalyst [52]. Promising catalysts, composed of NiCuCo-S and NiCu-N-C, for efficient NH_3 mineralization (~80% and > 90%) were reported by Wang et al. [66] and Zhang et al. [80]. As Fig. 9(a) show, addition of Co and S to a NiCu composite inhibited side reactions, thus the selectivity of N_2 evolution increased as follows NiCu < NiCu-S < NiCuCo-S. For comparison, NiCo oxide composites on Ni foam were prepared by precipitation followed by chemical oxidation or calcination by Shih et al. [74]. The highest selectivity of N_2 formation (40%) was achieved for the sample at equimolar ratio of Ni and Co (0.1 M Na_2SO_4 + 50 mg-N/L NH_3, pH 9–9.5, Fig. 10).

As presented, the effect of pH on the N_2 selectivity still remains disputable. For the single-metal (Ni)-based electrocatalyst, increase of the N_2 selectivity with pH was observed by Shih *et al* [59], while Medvedev et al. [50] reported the opposite relation. On the other hand, the double-metal (NiCu)-based electrocatalysts favor N_2 formation at lower pH [52,68].

Analyzing the results described above, the ammonia oxidation on Ni begins at potentials about 1.3 V and, as published data indicate [62,84], selective N_2 evolution is possible at potentials below 1.55 V *vs.* RHE. Exceeding this value leads to the formation of oxygenated forms of nitrogen [50]. However, the cyclic voltammetry experiments show steep increase in the current and we do not see changes in the run of the curve, *e.g.*, a peak or a wave, reflecting the crucial steps of ammonia oxidation, *i.e.* dehydrogenation according to the scheme shown in Fig. 1 and hydroxylation shown in Fig. 7. The reason may be the proximity of the potentials at which the various processes occur [58] or the differences in the mechanisms of AOR at Ni and Pt. It seems that at low potentials, the dehydrogenation of ammonia prevails over hydroxylation of $NH_{x,ads}$, *e.g.* on β-NiOOH with OH/O vacancies potentials of N_2 formation are lower than that of NO_2^- formation and equal to 1.12 V/0.97 V and 1.29 V/1.17 V *vs.* RHE, respectively [58]. This issue requires further clarification, in particular it is necessary to establish the role of water/OH^- or Ni hydroxide' oxygen lattice.

On the other hand, in the case of AOR at Pt, there is an apparent separation of the potential reflecting oxidation of NH_3 to N_2 (0.5–0.6 V *vs.* RHE) from NH_3 conversion to nitrites and nitrates at higher potentials (oxidation of N_{ads} to NO_x occur at ~1.0 V *vs.* RHE) [11,33]. At the onset potential of 0.5–0.6 V, atomic nitrogen adsorbs on the surface of the catalyst, and undergoes dimerization and desorption (we observe an increase in current density on the CV curve). The degree of surface coverage by N_{ads} systematically increases. It is likely, however, that the rate of N_{ads} adsorption (and thus the coverage of the blocked surface) is greater than the rate of the dimerization and N_2 desorption. For this reason, a decrease in current density was observed in the CV curve (*e.g.*, 0.62 V at [11]). Once a competitive reaction occurred, the evolution of N_2 was hindered.

2.5. Hydrogen production

Hydrogen production coupled with ammonia oxidation to nitrogen was reported for electrolytic cells with Pt-based electrodes at cell potentials as low as 0.5–0.6 V [85–87]. In the case of the currently known Ni-based electrocatalysts it is not possible to produce hydrogen at the potentials below 1.2–1.3 V [65,66] due to the aforementioned Ni^{2+} to Ni^{3+} conversion. Latvyte et al. [67] used electrolyzer containing NiCu/

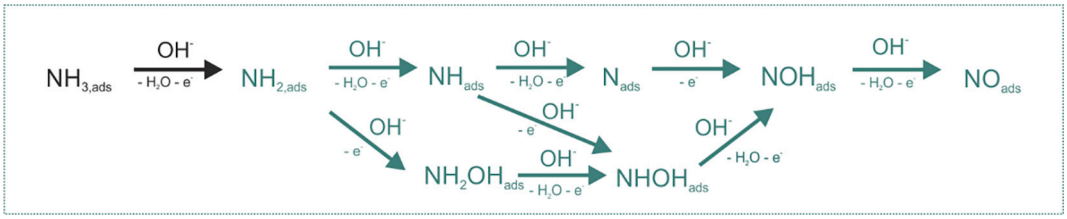

Fig. 7. Postulated mechanism of ammonia oxidation to nitrogen oxides based on the computational data [11,58].

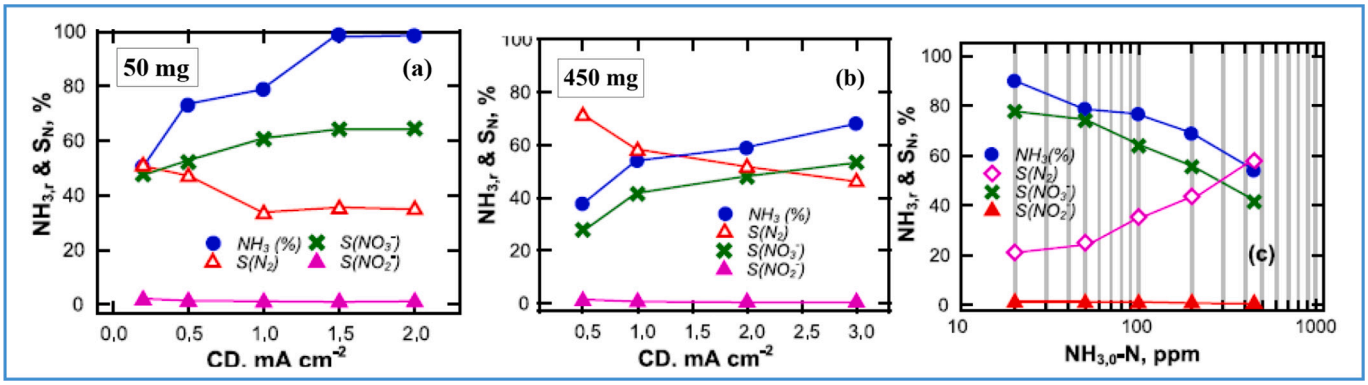

Fig. 8. Effect of current density and NH_3 concentration on the efficiency and selectivity of ammonia oxidation (adapted from [59]).

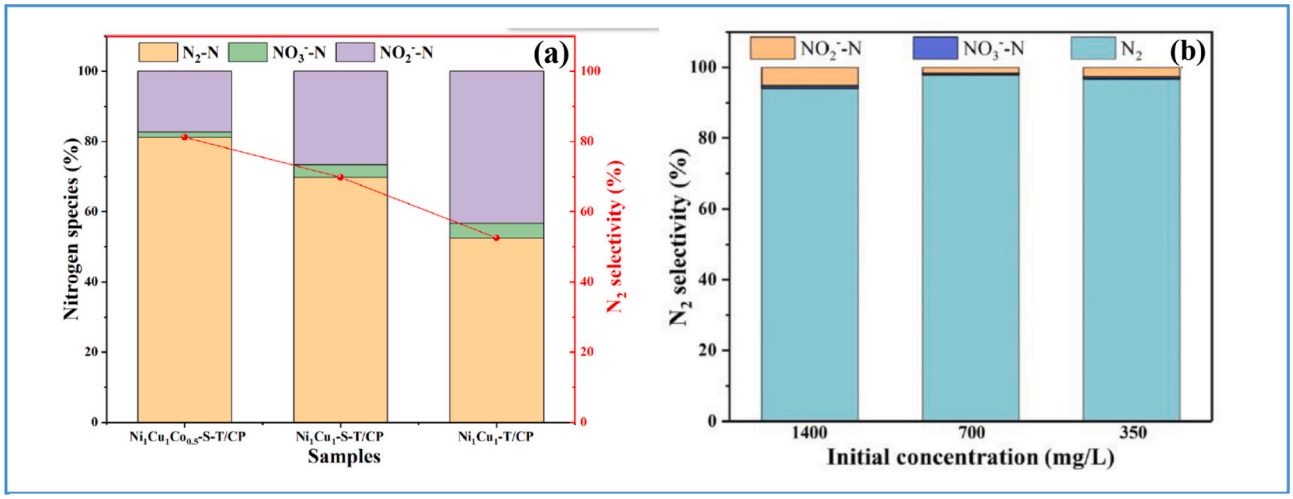

Fig. 9. Nitrogen selectivity of ammonia electrooxidation analyzed for the samples composed of (a) NiCuCo-S (adapted from [66]) and (b) NiCu-N-C (adapted from [80]) at potential 1.5 V.

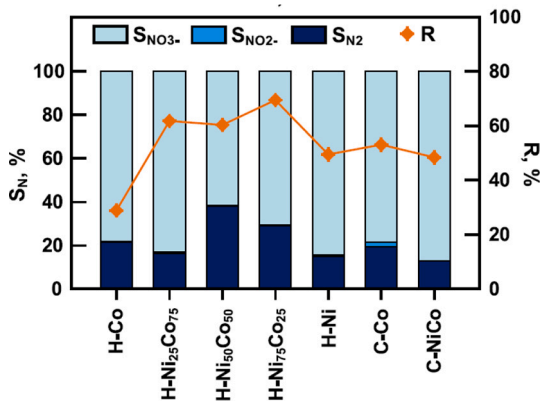

Fig. 10. Nitrogen selectivity of ammonia electrooxidation analyzed for the NiCo oxides composites, H denotes oxidation by sodium hypochlorite and C – calcination (j = 1.5 mA/cm^2) [74].

nickel felt anode and commercial NiFeCu cathode separated by an anion exchange membrane (Fig. 11a). The electrolysis experiments were conducted at constant currents and the measured voltages were highly dependent on the concentration of NH_3. For 0.3 M and 1.0 M of NH_3, the cell voltage at 200 mA/cm^2 was 1.90 V and 1.81 V, respectively (Fig. 11b). A long-term experiment at 100 mA/cm^2 showed the electrode maintained a stable ammonia oxidation rate (0.011 M/h) and high Faradaic efficiencies of >85% for at least 50 h at 20 °C. Apart from N_2 (total selectivity was 85.8%), the gas mixture evolved on the anode also contained O_2 (4.3%), H_2 (2.8%) and nitrous oxide (0.1%). Moreover, the nitrite and nitrate were also detected (2.3% for NO_3^- and 11.9% for NO_2^-). On the cathode hydrogen with purity of 99.6% was evolved.

There are other publications (a few) which titles read the studies were devoted to the ammonia electrolysis, but the texts lack data on the operation of the electrolytic cell *i.e.,* the amount and composition of the gases evolved, the efficiency of electrolysis, *etc.* They focus mainly on the oxidation reaction of NH_3. In this regard, more research is needed to elucidate the relationship between N_2 evolution or its further oxidation and H_2 production.

3. Conclusions

It is expected that breakthrough in the ammonia oxidation will be beneficial for energy conversion, its storage, electrochemical sensing, and wastewater treatment.

Ammonia is a carbon-free energy carrier, therefore could be used as on-board fuel for a vehicle using direct or indirect ammonia cells. Hydrogen necessary for indirect fuel cells can be produced by thermal decomposition NH_3 or its electrolysis in an aqueous solution with simultaneous release of nitrogen. The volumetric H_2 density in liquid ammonia is 12.1 kg/100 dm^3 (0.1 MPa, -33 °C), which is 1.7 times higher than that of liquid H_2 (7.08 kg/100 dm^3, 0.1 MPa, -253 °C). The electrolytic decomposition of ammonia requires less energy input (ΔG = 17.4 kJ/mol) than the electrolytic decomposition of water (ΔG

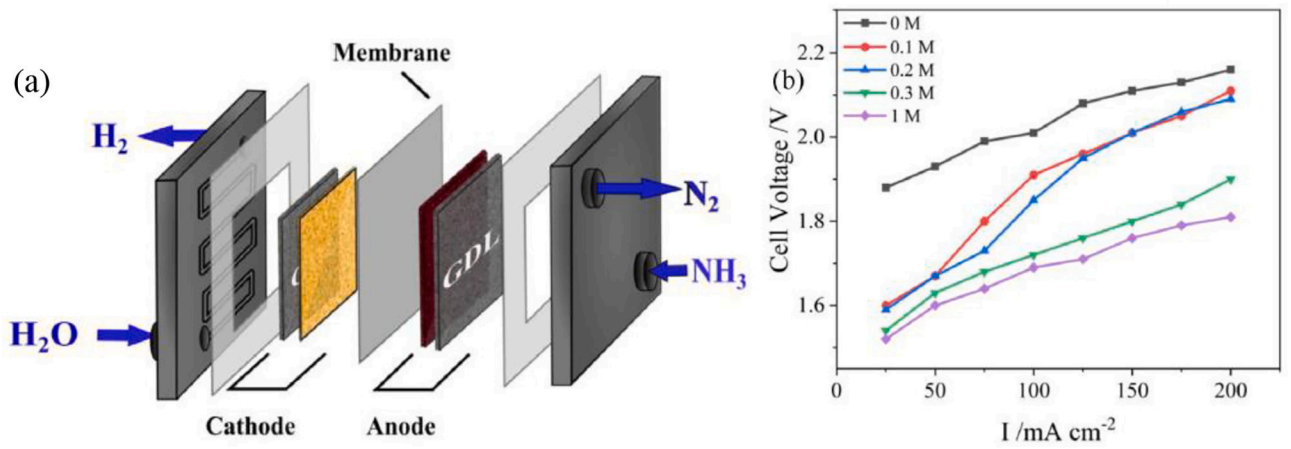

Fig. 11. (a) Electrolytic cell used by Latvyte et al. [67] for $NH_{3,aq}$ electrolysis; (b) cell voltage dependence on the concentration of ammonia in the KOH electrolyte, recorded at 20 °C.

= 237.3 kJ/mol).

The development of ammonia electrooxidation technology is hindered by the lack of efficient, cheap, and durable catalysts. The state-of-the-art catalysts for this process are still the traditional noble metals, such as Pt, Ir, and Ru, with prohibitive cost, low natural abundance, and proneness to poisoning, which are undesirable for sustainable energy-related applications in the future. Therefore, current studies are focused on the development of novel, low cost, and durable nickel-based catalysts, mainly oxides/hydroxides. As a result of the electrochemical processing, the surface reconstruction of Ni oxides and hydroxides takes place with the formation of NiOOH, which is believed to be the real center for the catalytic oxidation of ammonia. The potential at which this transformation occurs is 1.30–1.35 V *vs.* RHE, thus considering $E^{o}_{NH_3/N_2} = -0.097$ V the overpotential of AOR is *ca.* 1.4 V. Studies show that oxygen is not yet released at this potential, although the onset potential of the water oxidation reaction is only 0.2–0.3 V higher. This has two consequences. One is a reduction in energy yield, and the other is the formation of noxious oxygenated forms of nitrogen.

Up to date conducted research are realized in the following directions:

(i) production of $Ni(OH)_2$ from Ni itself (electrochemical oxidation of the Ni surface by the long-term cyclic voltammetry) or chemical coating of various substrates with Ni oxides/hydroxides,

(ii) modification of Ni-based materials with:

- free metals (*e.g.* Cu, Pd, Ag),
- nonmetals (*e.g.* S, P),
- metal's oxides/hydroxides (*e.g.* CuO, Co_2O_3).

The onset potential of the ammonia oxidation on the $Ni(OH)_2$/NiOOH redox couple without dopants was shown to be ~1.3–1.4 V *vs.* RHE. During the ammonia oxidation process NiOOH is reversibly reduced to $Ni(OH)_2$. The systems composed of $Ni(OH)_2$ with embedded Cu in various oxidation states seems to be most promising. An increase in the current density (from ~20 to ~90 mA/cm^2 at 1.5–1.6 V *vs.* RHE) was obtained. Unfortunately, catalytic activity of Cu on its own has not been proved yet, what hinders elucidation of its mode of action. The experimental or theoretical evidence for the potential catalytic activity of Cu(II) and Cu(I) are also still scarce and needs further studies.

The mechanism of ammonia oxidation on Ni is very poorly understood. Typically, researchers assume that the reaction proceeds analogously to that on Pt. However, the poisoning of the Ni surface due to adsorption of N atoms was not reported. At potentials higher than 1.5 V an unacceptable, from the environmental point of view, low selectivity of N_2 formation was revealed. A further drop of the N_2 selectivity was detected at even higher anodic potentials. Most authors tend to conclude that AOR on Ni follows the Gerischer-Maurer mechanism. However, recent studies show that the formation of oxidized forms of nitrogen is due to hydroxylation of $NH_{x,ads}$ ($x = 0 \div 2$) formed at all stages of dehydrogenation of NH_3. This means that the dimerization of $NH_{x,ads}$ ($x = 1 \div 2$) leading to the release of N_2 could run in parallel with the formation of oxidized forms of nitrogen.

4. Future perspectives

Challenges for future research:

(i) increasing the selectivity of the ammonia oxidation to N_2;

This could be achieved by the directing the reaction pathway towards the formation of NH_x-$NH_{x,ads}$ (the G-M mechanism), because it was shown in many reports that hydrazine electrooxidation undergoes with 100% selectivity.

(ii) lowering the overpotential of the ammonia oxidation reaction (thermodynamic parameter), which involves increasing the energy yield;

The binding energy of the hydrogen atom with the catalytic center (electron coupled proton transfer) should be higher than the energy of the H—N bonding.

(iii) increase in catalytic activity (kinetic parameter) enabling production of hydrogen similarly to that in conventional water oxidation process

It seems that increasing the level of technological readiness of AOR will be possible provided 200 mA/cm^2 current densities are achieved (lower current limit of the commercial electrolysis) at electrolysis voltages not exceeding the ones sufficient for water oxidation and formation of oxygenated forms nitrogen. Typical alkaline electrolyzes operate at 65-100 °C. At a similar temperature range, it is not possible to obtain the comparable hydrogen yields due to the limited solubility of ammonia in water (Table 3). Solubility of NH_3 in 100 g water at 20 °C, 30 °C, 40 °C and 50 °C is 54.5 g, 41.6 g, 31.5 g, 23.5 g, 16.7 g, respectively.

(iv) increasing the stability of the catalyst

It would be necessary to achieve such a modification of the electrocatalysts, for which the reversible conversion of the α-$Ni(OH)_2$ form

Table 3
Approximate hydrogen yield (kg H_2/100kg solution) of ammonia aqueous solution electrolysis at various temperatures regarding solubility of ammonia in water.

	20 °C	30 °C	40 °C	50 °C	60 °C
	kg H_2/100 kg solution				
NH_3 solution	6.2	5.2	4.2	3.4	2.5
H_2O	10				

to γ-NiOOH is maintained while blocking the conversion to β phases. The transformations of α-$Ni(OH)_2$ into β-$Ni(OH)_2$ and β-NiOOH to γ-NiOOH are associated with the transport of water and ions, which may hinder access of ammonia molecules to the active sites.

Research problems to be solved:

(i) Activity od the oxyhydroxide active layer on the Ni electrode could be hindered by adsorbed N and NO_x. There are no data on the adsorption energy of NH_x, N, NO_x on the Ni surface covered with (hydro)oxides.
(ii) NiOOH layer as a semiconductor inhibits swift charge transfer across the interface, therefore its conductivity should be improved by converting the layer into composite by depositing conductive nanoadditives like copper, graphene *etc.*
(iii) Ni-based catalysts should be endowed to not catalyze oxygen evolution to increase current efficiency of ammonia oxidation.
(iv) It is necessary to establish the mechanism and parameters which determine the formation of NO_x, NO_2^- or NO_3^- to maximize the selectivity of N_2 evolution. Due to low N_2 selectivity, nitrogen oxoanions may accumulate in the solution on prolonged electrolysis that is why its influence on the Ni oxides activity might be detrimental. This issue must be clarified.

Declaration of Competing Interest

The authors declare the following financial interests/personal relationships which may be considered as potential competing interests:

Justyna Luczak, Marek Lieder reports financial support was provided by National Science Centre Poland.

Data availability

The Authors have permissions to share data

Acknowledgment

This research was supported by the National Science Center Poland under the grant 2021/41/B/ST4/03255.

References

[1] Bard AJ, Parsons R, Jordan J. Standard potentials in aqueous solution. Routledge; 1985 [ISBN 9780203738764.].
[2] Jeerh G, Zhang M, Tao S. Recent progress in ammonia fuel cells and their potential applications. J Mater Chem A 2021;9:727–52.
[3] López De Mishima BA, Lescano D, Molina Holgado T, Mishima HT. Electrochemical oxidation of ammonia in alkaline solutions: its application to an amperometric sensor. Electrochim Acta 1998;43:395–404. https://doi.org/10.1016/S0013-4686(97)00061-3.
[4] Feng C, Sugiura N, Shimada S, Maekawa T. Development of a high performance electrochemical wastewater treatment system. J Hazard Mater 2003;103:65–78. https://doi.org/10.1016/S0304-3894(03)00222-X.
[5] Despić AR, Dražić DM, Rakin PM. Kinetics of electrochemical oxidation of ammonia in alkaline solution. Electrochim Acta 1966;11:997–1005. https://doi.org/10.1016/0013-4686(66)80038-5.
[6] Oswin HG, Salomon M. The anodic oxidation of ammonia at platinum black electrodes in aqueous KOH electrolyte. Can J Chem 1963;41:1686–94. https://doi.org/10.1139/v63-243.
[7] Rosca V, Koper MTM. Electrocatalytic oxidation of ammonia on Pt(111) and Pt (100) surfaces. Phys Chem Chem Phys 2006;8:2513–24. https://doi.org/10.1039/B601306F.
[8] Gerischer H, Mauerer A. Untersuchungen Zur anodischen Oxidation von Ammoniak an Platin-Elektroden. J Electroanal Chem Interfacial Electrochem 1970;25:421–33. https://doi.org/10.1016/S0022-0728(70)80103-6.
[9] Matsui T, Suzuki S, Katayama Y, Yamauchi K, Okanishi T, Muroyama H, et al. *In situ* attenuated total reflection infrared spectroscopy on electrochemical ammonia oxidation over Pt electrode in alkaline aqueous solutions. Langmuir 2015;31:11717–23. https://doi.org/10.1021/acs.langmuir.5b02330.
[10] Herron JA, Ferrin P, Mavrikakis M. Electrocatalytic oxidation of Ammonia on transition-metal surfaces: a first-principles study. J Phys Chem C 2015;119:14692–701. https://doi.org/10.1021/jp512981f.
[11] Katsounaros I, Figueiredo MC, Calle-Vallejo F, Li H, Gewirth AA, Markovic NM, et al. On the mechanism of the electrochemical conversion of ammonia to dinitrogen on Pt(100) in alkaline environment. J Catal 2018;359:82–91. https://doi.org/10.1016/J.JCAT.2017.12.028.
[12] McBreen J. Nickel hydroxides. In: Handbook of battery materials. John Wiley & Sons, Ltd; 2011. p. 149–68 [ISBN 9783527637188.].
[13] Angeles-Olvera Z, Crespo-Yapur A, Rodríguez O, Cholula-Díaz J, Martínez L, Videa M. Nickel-based electrocatalysts for water electrolysis. Energies 2022;15:1609. https://doi.org/10.3390/en15051609.
[14] Siddharth K, Chan Y, Wang L, Shao M. Ammonia electro-oxidation reaction: recent development in mechanistic understanding and electrocatalyst design. Curr Opin Electrochem 2018;9:151–7. https://doi.org/10.1016/J.COELEC.2018.03.011.
[15] Tian, Y.; Mao, Z.; Wang, L.; Liang, J. Green chemistry: advanced electrocatalysts and system design for ammonia oxidation. Small Struct *n/a*, 2200266, doi: https://doi.org/10.1002/sstr.202200266.
[16] Zhong C, Hu WB, Cheng YF. Recent advances in electrocatalysts for electro-oxidation of ammonia. J Mater Chem A 2013;1:3216–38. https://doi.org/10.1039/C2TA00607C.
[17] Guo W, Zhang K, Liang Z, Zou R, Xu Q. Electrochemical nitrogen fixation and utilization: theories{,} advanced catalyst materials and system design. Chem Soc Rev 2019;48:5658–716. https://doi.org/10.1039/C9CS00159J.
[18] Xi X, Fan Y, Zhang K, Liu Y, Nie F, Guan H, et al. Carbon-free sustainable energy technology: Electrocatalytic ammonia oxidation reaction. Chem Eng J 2022;435:134818. https://doi.org/10.1016/J.CEJ.2022.134818.
[19] Afif A, Radenahmad N, Cheok Q, Shams S, Kim JH, Azad AK. Ammonia-fed fuel cells: a comprehensive review. Renew Sustain Energy Rev 2016;60:822–35. https://doi.org/10.1016/J.RSER.2016.01.120.
[20] Adli NM, Zhang H, Mukherjee S, Wu G. Review—Ammonia oxidation Electrocatalysis for hydrogen generation and fuel cells. J Electrochem Soc 2018;165:J3130–47. https://doi.org/10.1149/2.0191815jes.
[21] Zhou B, Zhang N, Wu Y, Yang W, Lu Y, Wang Y, et al. An option for green and sustainable future: electrochemical conversion of ammonia into nitrogen. J Energy Chem 2021;60:384–402. https://doi.org/10.1016/J.JECHEM.2021.01.011.
[22] Vanderzee CE, King DL. The enthalpies of solution and formation of ammonia. J Chem Thermodyn 1972;4:675–83. https://doi.org/10.1016/0021-9614(72)90039-0.
[23] Diawara B, Joubert L, Costa D, Marcus P, Adamo C. Ammonia on Ni(111) surface studied by first principles: bonding, multilayers structure and comparison with experimental IR and XPS data. Surf Sci 2009;603:3025–34. https://doi.org/10.1016/j.susc.2009.08.001.
[24] Chattopadhyay A, Yang H, Whitten L. Adsorption of ammonia on nickel(111). J Phys Chem 2002;94:6379–83. https://doi.org/10.1021/j100379a042.
[25] Yin H, Qiu Y-P, Dai H, Gan L-Y, Dai H-B, Wang P. Understanding of selective H2 generation from hydrazine decomposition on Ni(111) surface. J Phys Chem C 2018;122:5443–51. https://doi.org/10.1021/acs.jpcc.7b11293.
[26] Novell-Leruth G, Valcárcel A, Clotet A, Ricart M, Pérez-Ramírez J. DFT characterization of adsorbed NHx species on Pt(100) and Pt(111) surfaces. J Phys Chem B 2005;109:18061–9. https://doi.org/10.1021/jp051682l.
[27] Liu Z-P, Hu P, Lee M-H. Insight into association reactions on metal surfaces: density-functional theory studies of hydrogenation reactions on Rh(111). J Chem Phys 2003;119:6282–9. https://doi.org/10.1063/1.1602054.
[28] Elnabawy AO, Herron JA, Karraker S, Mavrikakis M. Structure sensitivity of ammonia electro-oxidation on transition metal surfaces: a first-principles study. J Catal 2021;397:137–47. https://doi.org/10.1016/J.JCAT.2021.03.010.
[29] Li H, Li Y, Koper TM, Calle-Vallejo F. Bond-making and breaking between carbon, nitrogen, and oxygen in electrocatalysis. J Am Chem Soc 2014;136:15694–701. https://doi.org/10.1021/ja508649p.
[30] Wallace SW, McCrum IT, Janik MJ. Ammonia electro-oxidation mechanism on the platinum (100) surface. Catal Today 2021;371:50–7. https://doi.org/10.1016/J.CATTOD.2020.09.024.
[31] Pillai HS, Xin H. New insights into electrochemical ammonia oxidation on Pt(100) from first principles. Ind Eng Chem Res 2019;58:10819–28. https://doi.org/10.1021/acs.iecr.9b01471.
[32] Novell-Leruth G, Ricart M, Pérez-Ramírez J. Pt(100)-catalyzed ammonia oxidation studied by DFT: mechanism and microkinetics. J Phys Chem C 2008;112:13554–62. https://doi.org/10.1021/jp802489y.
[33] De Vooys ACA, Koper MTM, Van Santen RA, Van Veen JAR. The role of adsorbates in the electrochemical oxidation of ammonia on noble and transition metal electrodes. J Electroanal Chem 2001;506:127–37. https://doi.org/10.1016/S0022-0728(01)00491-0.
[34] Choueiri RM, Tatarchuk SW, Klinkova A, Chen LD. Mechanism of ammonia oxidation to dinitrogen, nitrite, and nitrate on β-Ni(OH)2 from first-principles

simulations. Electrochem Sci Adv 2021;2:2100142. https://doi.org/10.1002/elsa.202100142.
[35] Hall DS, Lockwood DJ, Bock C, MacDougall BR. Nickel hydroxides and related materials: a review of their structures, synthesis and properties. Proc R Soc A Math Phys Eng Sci 2015;471:20140792. https://doi.org/10.1098/rspa.2014.0792.
[36] Huang L-F, Hutchison J, Santucci Jr J, Scully R, Rondinelli M. Improved electrochemical phase diagrams from theory and experiment: the Ni–water system and its complex compounds. J Phys Chem C 2017;121:9782–9. https://doi.org/10.1021/acs.jpcc.7b02771.
[37] Kapalka A, Cally A, Neodo S, Comninellis C, Wächter M, Udert KM. Electrochemical behavior of ammonia at Ni/Ni(OH)2 electrode. Electrochem Commun 2010;12:18–21. https://doi.org/10.1016/j.elecom.2009.10.026.
[38] Fleischmann M, Korinek K, Pletcher D. The oxidation of organic compounds at a nickel anode in alkaline solution. J Electroanal Chem Interfacial Electrochem 1971;31:39–49. https://doi.org/10.1016/S0022-0728(71)80040-2.
[39] Smith RJ, Hummel RE, Ambrose JR. The passivation of nickel in aqueous solutions—II. An in situ investigation of the passivation of nickel using optical and electrochemical techniques. Corros Sci 1987;27:815–26. https://doi.org/10.1016/0010-938X(87)90039-4.
[40] Zhang L, Macdonald DD. Segregation of alloying elements in passive systems—I. XPS studies on the Ni–W system. Electrochim Acta 1998;43:2661–71. https://doi.org/10.1016/S0013-4686(97)00268-5.
[41] Oblonsky LJ, Devine TM. Surface enhanced Raman spectra from the films formed on nickel in the passive and Transpassive regions. J Electrochem Soc 1995;142:3677–82. https://doi.org/10.1149/1.2048398.
[42] Motori A, Sandrolini F, Davolio G. Electrical properties of nickel hydroxide for alkaline cell systems. J Power Sources 1994;48:361–70. https://doi.org/10.1016/0378-7753(94)80032-4.
[43] Bode H, Dehmelt K, Witte J. Zur kenntnis der nickelhydroxidelektrode—I.Über das nickel (II)-hydroxidhydrat. Electrochim Acta 1966;11:1079–87. https://doi.org/10.1016/0013-4686(66)80045-2.
[44] Aghazadeh M, Ghaemi M, Sabour B, Dalvand S. Electrochemical preparation of α-Ni(OH)2 ultrafine nanoparticles for high-performance supercapacitors. J Solid State Electrochem 2014;18:1569–84. https://doi.org/10.1007/s10008-014-2381-7.
[45] Klaus S, Cai Y, Louie W, Trotochaud L, Bell A. Effects of Fe electrolyte impurities on Ni(OH)2/NiOOH structure and oxygen evolution activity. J Phys Chem C 2015;119:7243–54. https://doi.org/10.1021/acs.jpcc.5b00105.
[46] Casella IG, Guascito MR, Sannazzaro MG. Voltammetric and XPS investigations of nickel hydroxide electrochemically dispersed on gold surface electrodes. J Electroanal Chem 1999;462:202–10. https://doi.org/10.1016/S0022-0728(98)00413-6.
[47] van Drunen J, Kinkead B, Wang CP, Sourty E, Gates B, Jerkiewicz G. Comprehensive structural, surface-chemical and electrochemical characterization of nickel-based metallic foams. ACS Appl Mater Interfaces 2013;5:6712–22. https://doi.org/10.1021/am401606n.
[48] Singh D. Characteristics and effects of γ-NiOOH on cell performance and a method to quantify it in nickel electrodes. J Electrochem Soc 1998;145:116–20. https://doi.org/10.1149/1.1838222.
[49] Häring P, Kötz R. Nanoscale thickness changes of nickel hydroxide films during electrochemical oxidation/reduction monitored by in situ atomic force microscopy. J Electroanal Chem 1995;385:273–7. https://doi.org/10.1016/0022-0728(94)03869-5.
[50] Medvedev JJ, Tobolovskaya Y, Medvedeva XV, Tatarchuk SW, Li F, Klinkova A. Pathways of ammonia electrooxidation on nickel hydroxide anodes and an alternative route towards recycled fertilizers. Green Chem 2022;24:1578–89. https://doi.org/10.1039/D1GC04140A.
[51] Doyle RL, Godwin IJ, Brandon MP, Lyons MEG. Redox and electrochemical water splitting catalytic properties of hydrated metal oxide modified electrodes. Phys Chem Chem Phys 2013;15:13737–83. https://doi.org/10.1039/C3CP51213D.
[52] Song J, Yinhai Y, Jia Y, Wang T, Wei J, Wang M, et al. Improved NH3-N conversion efficiency to N2 activated by BDD substrate on NiCu electrocatalysis process. Sep Purif Technol 2021;276:119350. https://doi.org/10.1016/J.SEPPUR.2021.119350.
[53] Chen W, Xie C, Wang Y, Zou Y, Dong CL, Huang YC, et al. Activity origins and design principles of nickel-based catalysts for nucleophile electrooxidation. Chem 2020;6:2974–93. https://doi.org/10.1016/j.chempr.2020.07.022.
[54] Zhao W, Carey J, Mao Z, Campbell C. Adsorbed hydroxyl and water on Ni(111): heats of formation by calorimetry. ACS Catal 2018;8:1485–9. https://doi.org/10.1021/acscatal.7b04041.
[55] Liu R, Shen W, Zhang J, Li M. Adsorption and dissociation of ammonia on au(111) surface: a density functional theory study. Appl Surf Sci 2008;254:5706–10. https://doi.org/10.1016/J.APSUSC.2008.03.031.
[56] Agusta MK, Purwoko PH, Saputro AG, Fathurrahman F, Dipojono HK, Diño WA. Conformational effects on hydrazine and OH coadsorption on Ni(111): a first-principles investigation. Surf Sci 2017;664:185–93. https://doi.org/10.1016/J.SUSC.2017.06.013.
[57] Zhang S, Yan L, Jiang H, Zhao Y, Yang L, Fu Q, et al. Modulating the coadsoption of hydroxyl and nitrogenous groups induced by Ni and Cu doping on FeOOH for accelerating dehydrogenation in the ammonia oxidation reaction. Sci China Mater 2023. https://doi.org/10.1007/s40843-022-2433-6.
[58] Choueiri M, R.; D, Chen L. Favorable electrocatalytic ammonia oxidation reaction thermodynamics on the β-NiOOH(0001) surface computed by density functional theory. J Phys Chem C 2022;126:17952–65. https://doi.org/10.1021/acs.jpcc.2c06174.
[59] Shih YJ, Huang YH, Huang CP. In-situ electrochemical formation of nickel oxyhydroxide (NiOOH) on metallic nickel foam electrode for the direct oxidation of ammonia in aqueous solution. Electrochim Acta 2018;281:410–9. https://doi.org/10.1016/J.ELECTACTA.2018.05.169.
[60] Almomani F, Bhosale R, Khraisheh M, Kumar A, Tawalbeh M. Electrochemical oxidation of ammonia on nickel oxide nanoparticles. Int J Hydrogen Energy 2020;45:10398–408. https://doi.org/10.1016/J.IJHYDENE.2019.11.071.
[61] Gonzalez-Reyna M, Luna-Martínez MS, Perez-Robles JF. Nickel supported on carbon nanotubes and carbon nanospheres for ammonia oxidation reaction. Nanotechnology 2020;31:235706. https://doi.org/10.1088/1361-6528/ab73b6.
[62] Huang J, Cai J, Wang J. Nanostructured wire-in-plate electrocatalyst for high-durability production of hydrogen and nitrogen from alkaline ammonia solution. ACS Appl Energy Mater 2020;3:4108–13. https://doi.org/10.1021/acsaem.9b02545.
[63] Xu W, Lan R, Du D, Humphreys J, Walker M, Wu Z, et al. Directly growing hierarchical nickel-copper hydroxide nanowires on carbon fibre cloth for efficient electrooxidation of ammonia. Appl Catal Environ 2017;218:470–9. https://doi.org/10.1016/J.APCATB.2017.07.005.
[64] Jiang X, Ying D, Liu X, Liu M, Zhou S, Guo C, et al. Identification of the role of cu site in Ni-cu hydroxide for robust and high selective electrochemical ammonia oxidation to nitrite. Electrochim Acta 2020;345:136157. https://doi.org/10.1016/J.ELECTACTA.2020.136157.
[65] Zhang H, Chen W, Wang H, Tong X, Wang Y, Yang X, et al. A core-shell NiCu@NiCuOOH 3D electrode induced by surface electrochemical reconstruction for the ammonia oxidation reaction. Int J Hydrogen Energy 2022;47:16080–91. https://doi.org/10.1016/j.ijhydene.2022.03.139.
[66] Wang H, Tong X, Zhou L, Wang Y, Liao L, Ouyang S, et al. Unique three-dimensional nanoflower-like NiCu electrodes constructed by Co, S co-doping for efficient ammonia oxidation reaction. Sep Purif Technol 2022;303:122293. https://doi.org/10.1016/J.SEPPUR.2022.122293.
[67] Latvytė E, Zhu X, Wu L, Lan R, Vale P, Graves JE. A low-temperature ammonia electrolyser for wastewater treatment and hydrogen production. Int J Hydrogen Energy 2023. https://doi.org/10.1016/J.IJHYDENE.2023.05.076.
[68] Tsai MH, Juang Y, Hu CC, Hua LC, Mahata BK, Huang C. The direct electrocatalytic oxidation of ammonia by copper-deposited nickel foam catalysts. Electrochim Acta 2023;446:142130. https://doi.org/10.1016/J.ELECTACTA.2023.142130.
[69] Prabowo Rahardjo SS, Shih Y-J. Electrocatalytic ammonia oxidation mediated by nickel and copper crystallites decorated with platinum nanoparticle (PtM/G, M = Cu, Ni). ACS Sustain Chem Eng 2022;10:5043–54. https://doi.org/10.1021/acssuschemeng.2c00740.
[70] Zhang HM, Wang YF, Kwok YH, Wu ZC, Xia DH, Leung DYC. A direct ammonia microfluidic fuel cell using NiCu nanoparticles supported on carbon nanotubes as an electrocatalyst. ChemSusChem 2018;11:2889–97. https://doi.org/10.1002/cssc.201801232.
[71] Zhang H, Wang H, Tong X, Zhou L, Yang X, Wang Y, et al. Sulfur induced surface reconfiguration of Ni1Cu3-S-T/CP anode for high-efficiency ammonia electro-oxidation. Chem Eng J 2023;452:139582. https://doi.org/10.1016/J.CEJ.2022.139582.
[72] Zhu M, Yang Y, Xi S, Diao C, Yu Z, Lee WSV, et al. Deciphering NH3 adsorption kinetics in ternary Ni–Cu–Fe oxyhydroxide toward efficient ammonia oxidation reaction. Small 2021;17:2005616. https://doi.org/10.1002/smll.202005616.
[73] Hu S, Tan Y, Feng C, Wu H, Zhang J, Mei H. Synthesis of N doped NiZnCu-layered double hydroxides with reduced graphene oxide on nickel foam as versatile electrocatalysts for hydrogen production in hybrid-water electrolysis. J Power Sources 2020;453:227872. https://doi.org/10.1016/J.JPOWSOUR.2020.227872.
[74] Shih YJ, Hsu CH. Kinetics and highly selective N2 conversion of direct electrochemical ammonia oxidation in an undivided cell using NiCo oxide nanoparticle as the anode and metallic Cu/Ni foam as the cathode. Chem Eng J 2021;409:128024. https://doi.org/10.1016/J.CEJ.2020.128024.
[75] Almomani F, Salah Ali H, Saad M. Electrochemical oxidation of ammonia (NH4+/NH3) ON synthesized nickel-cobalt oxide catalyst. Int J Hydrogen Energy 2021;46:4678–90. https://doi.org/10.1016/J.IJHYDENE.2020.03.094.
[76] Rahardjo SSP, Shih YJ. Electrochemical characteristics of silver/nickel oxide (Ag/Ni) for direct ammonia oxidation and nitrogen selectivity in paired electrode system. Chem Eng J 2023;452:139370. https://doi.org/10.1016/J.CEJ.2022.139370.
[77] Allagui A, Sarfraz S, Baranova EA. NixPd1− (x= 0.98, 0.93, and 0.58) nanostructured catalysts for ammonia electrooxidation in alkaline media. Electrochim Acta 2013;110:253–9. https://doi.org/10.1016/j.electacta.2013.06.148.
[78] Vidal-Iglesias FJ, Solla-Gullón J, Montiel V, Feliu JM, Aldaz A. Screening of electrocatalysts for direct ammonia fuel cell: Ammonia oxidation on PtMe (Me: Ir, Rh, Pd, Ru) and preferentially oriented Pt(100) nanoparticles. J Power Sources 2007;171:448–56. https://doi.org/10.1016/j.jpowsour.2007.06.015.
[79] Wang R, Liu H, Zhang K, Zhang G, Lan H, Qu J. Ni(II)/Ni(III) redox couple endows Ni foam-supported Ni2P with excellent capability for direct ammonia oxidation. Chem Eng J 2021;404:126795. https://doi.org/10.1016/j.cej.2020.126795.
[80] Zhang H, Wang H, Zhou L, Li Q, Yang X, Wang Y, et al. Efficient and highly selective direct electrochemical oxidation of ammonia to dinitrogen facilitated by NiCu diatomic site catalysts. Appl Catal Environ 2023;328:122544. https://doi.org/10.1016/J.APCATB.2023.122544.
[81] Zhang H, Wang Y, Wu Z, Leung DYC. An ammonia electrolytic cell with NiCu/C as anode catalyst for hydrogen production. Energy Procedia 2017;142:1539–44. https://doi.org/10.1016/J.EGYPRO.2017.12.605.
[82] Xu W, Du D, Lan R, Humphreys J, Miller DN, Walker M, et al. Electrodeposited NiCu bimetal on carbon paper as stable non-noble anode for efficient

electrooxidation of ammonia. Appl Catal Environ 2018;237:1101–9. https://doi.org/10.1016/J.APCATB.2016.11.003.
[83] Wang Y, Li T, Yu Y, Zhang B. Electrochemical synthesis of nitric acid from nitrogen oxidation. Angew Chem Int Ed 2022;61:e202115409. https://doi.org/10.1002/anie.202115409.
[84] Shih Y-J, Huang Y-H, Huang CP. Electrocatalytic ammonia oxidation over a nickel foam electrode: role of Ni(OH)2(s)-NiOOH(s) nanocatalysts. Electrochim Acta 2018;263:261–71. https://doi.org/10.1016/j.electacta.2018.01.045.
[85] Jiang M, Zhu D, Zhao X. Electrolysis of ammonia for hydrogen production catalyzed by Pt and Pt-Ir deposited on nickel foam. J Energy Chem 2014;23:1–8. https://doi.org/10.1016/S2095-4956(14)60110-8.
[86] Zhou Y, Zhang G, Yu M, Wang X, Lv J, Yang F. Free-standing 3D porous N-doped graphene aerogel supported platinum nanocluster for efficient hydrogen production from ammonia electrolysis. ACS Sustain Chem Eng 2018;6:8437–46. https://doi.org/10.1021/acssuschemeng.8b00586.
[87] Yang Y, Kim J, Jo H, Seong A, Lee M, Min H-K, et al. A rigorous electrochemical ammonia electrolysis protocol with in operando quantitative analysis. J Mater Chem A 2021;9:11571–9. https://doi.org/10.1039/D1TA00363A.